Quantitative Analysis and Visualized Evidence for High Charge Separation Efficiency in a Solid-Liquid Bulk Heterojunction

Xin Zhao, Wenjun Luo, Jianyong Feng, Mingxue Li, Zhaosheng Li, Tao Yu, and Zhigang Zou**

In the past few decades, some novel low-cost nanostructured devices have been explored for converting solar energy into electrical or chemical energy, such as organic photovoltaic cells, photoelectrochemical solar cells, and solar water splitting cells. Generally, higher light absorption and/or charge separation efficiency are considered as the main reasons for improved performance in a nanostructured device versus a planar structure. However, quantitative analysis and definite experimental evidence remain elusive. Here, using $BiVO_4$ as an example, comparable samples with porous and dense structures have been prepared by a simple method. The porous and dense films are assembled into a solid-electrolyte bulk and planar heterojunction, respectively. Some quantitative results are obtained by decoupling photon absorption, interfacial charge transfer, and charge separation processes. These results suggest that higher charge separation efficiency is mainly responsible for enhanced performance in a solid-electrolyte bulk heterojunction. Moreover, we also present visualized evidence to show higher charge separation efficiency comes from a shorter photo-generated hole diffusion distance in a bulk heterojunction. These results can deepen understanding charge transfer in a bulk heterojunction and offer guidance to design a more efficient low-cost device for solar conversion and storage.

1. Introduction

Solar energy is considered as the most promising renewable and clean energy resource to meet the challenge of fossil energy shortage and serious environmental issues. A conventional photovoltaic (PV) cell (using, for example, silicon or gallium arsenide), though capable of achieving a high conversion efficiency, faces the main obstacle of high cost for large-scale application because of the requirement of high purity and low defect density.

In the past few decades, some novel cells of low cost have been explored to convert solar energy into electrical or chemical energy, such as organic photovoltaic cells (OPV), photoelectrochemical solar cells, and photoelectrochemical solar water splitting cells.[1–5] In these devices, a key limit in a planar structure cell for high efficiency is the incompatibility between a short diffusion length of minority carriers and a long optical absorption length. To overcome the limit, bulk heterojunction (BHJ) concept is first introduced in an OPV cell,[6] which consists of an interpenetrating network of donor and acceptor materials.[7,8] The performance of the BHJ solar cell depends on the morphology very sensitively. A large interface area is usually necessary for high separation efficiency. In a photoelectrochemical solar cell or water splitting cell, one-dimensional nanostructure (nanowires, nanorods, or nanotubes),[9–12] branched nanostructure,[13,14] and porous structures,[15–19] are used to increase light capture and decrease diffusion distance of minority carriers to the interface. In a nanostructured photoelectrochemical cell, electrolyte can penetrate into the bulk of a solid photoelectrode. Therefore, analogically, a nanostructured photoelectrochemical cell can be considered as a solid-electrolyte bulk heterojunction.

Generally, higher light absorption and/or charge separation efficiency are considered as the main reasons for improved performance in a nanostructured cell than a planar structure. However, quantitative analysis and definite experimental evidence remain elusive. It is difficult to directly compare a nanostructured cell with a planar cell because the controlled samples are usually prepared by different methods or different conditions. Especially, in an OPV, it is difficult to investigate the details once the cell is assembled and a solid-solid interface forms. Therefore, it is impossible to identify quantitative contribution of each factor. Only some qualitative conclusions are given in previous studies.

X. Zhao,[+] Dr. W. Luo,[+] M. Li, Prof. T. Yu, Prof. Z. Zou
Eco-materials and Renewable Energy
Research Center (ERERC)
National Laboratory of Solid State Microstructures
and Department of Physics
Nanjing University
Nanjing 210093, P.R. China
E-mail: wjluo@nju.edu.cn; zgzou@nju.edu.cn

J. Feng, Prof. Z. Li
College of Engineering and Applied Science
Nanjing University
Nanjing 210093, P.R. China

[+]These authors contributed equally to this work.

DOI: 10.1002/aenm.201301785

In this study, using $BiVO_4$ as an example, samples with porous and planar structures are prepared under similar conditions by a very simple method. The porous and the dense films are assembled into a solid-electrolyte bulk heterojunction and a planar heterojunction, respectively. The two samples can be compared as they have similar crystallinity and impurity concentrations. Some quantitative results are obtained by decoupling photon absorption, interfacial charge transfer, and charge separation efficiency. Moreover, we present visualized evidence for hole transport by using Mn^{2+} as a hole imaging agent. These results can deepen understanding on charge transport in a nanostructure device and provide reference to designing a higher efficiency device for solar conversion and storage.

2. Results and Discussion

2.1. Comparison of Photoelectrochemical Performance Between a Solid/Electrolyte BHJ and a Planar Structure

Porous and dense 3% Mo doped $BiVO_4$ films are synthesized in this study. XPS and Raman data suggest that Mo ions are doped into $BiVO_4$ lattices successfully (Figure S1, Supporting Information). The typical morphologies of these two structures are presented in **Figure 1**. The porous film is composed of tightly connected wormlike particles with amounts of void spaces in a size of 100–200 nm shown in Figure 1a, which is comparable to our previous work.[19] Figure 1b shows the surface structure of the dense film prepared layer by layer, which consists of small particles with size of about 100–200 nm. The particles are strongly connected and void space is hardly observed. The cross-section SEM images of the porous and dense films are also presented in Figure 1c and Figure 1d, respectively. Obvious pores throughout the entire film can be seen for the porous film in Figure 1c, whereas the dense film is composed of a compact layer with no pores in the bulk (Figure 1d).

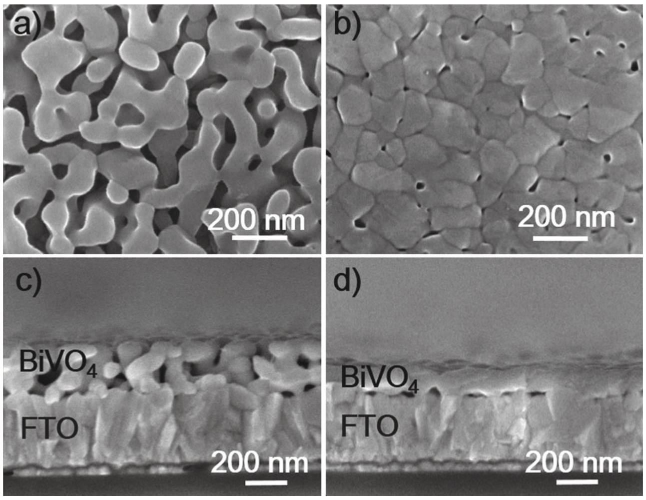

Figure 1. Top view SEM images of a) a porous Mo doped $BiVO_4$ film and b) a dense Mo doped $BiVO_4$ film. Cross-section SEM images of c) a porous Mo doped $BiVO_4$ film and d) a dense Mo doped $BiVO_4$ film.

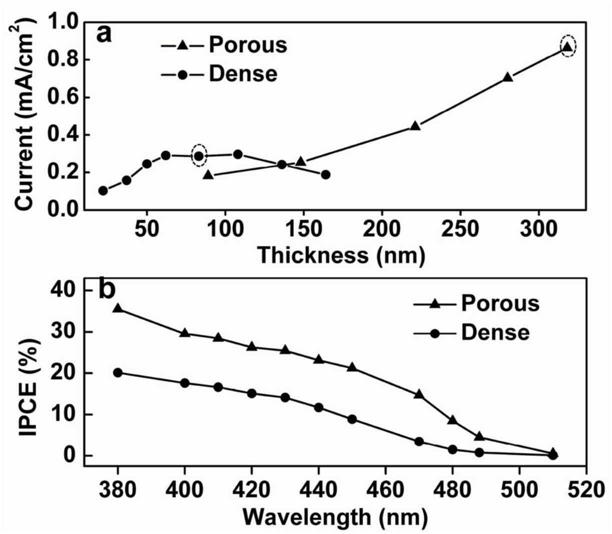

Figure 2. a) The photocurrent at 1.23 V_{RHE} of the porous and the dense Mo doped $BiVO_4$ films with different thickness in 0.5 M Na_2SO_4 aqueous solution under front (electrolyte-$BiVO_4$ surface side) illumination with a 500 W Xe lamp equipped with a 420 nm cut-off filter at a scan rate of 30 mV s^{-1}. b) Incident photon to current efficiency (IPCE) at 1.23 V_{RHE} of the porous and the dense $BiVO_4$ films (framed in Figure 2a) in 0.5 M Na_2SO_4 aqueous solution under front illumination.

The morphology of the Mo doped $BiVO_4$ film was tuned by changing the volume of the precursor solution and dropping layers. A single layer film is of pore structure no matter how thin it is. While, if the film is prepared with multi-layers, the pores in the first layer will be filled by the following layer. Therefore, a dense film is obtained. Porous and dense films with different thickness are obtained in our experiments (Figure S2, Supporting Information). Generally, some inevitable changes are present in a dense and a porous film, which will influence the comparison of the photoelectrochemical property contributed by the structure.[20,21] In this study, all the samples are prepared by the same method on similar conditions, which minimizes the difference except the morphology. Only possible difference is sample crystallinity due to different calcining time. To exclude this difference, all the samples were finally calcined at 470 °C for 5 h. XRD patterns of the porous and the dense films (Figure S3, Supporting Information) suggest that both the samples have similar crystallinity.

In general, one can investigate the effect of porous structure on the performance of photoanodes with the same thickness. However, photoelectrochemical performance depends on the film thickness very sensitively. To systematically evaluate the effect of pore structure, the photocurrents for water splitting of the porous and the dense $BiVO_4$ films with different thickness were investigated in this study. The results are shown in **Figure 2**a. For the dense film, the photocurrent increases firstly and then decreases with increasing thickness. However, for the porous film, the photocurrent increases with increasing thickness. A thicker porous film cannot be obtained by dropping one layer due to extravasation of the solution from the FTO substrate. The porous films with the thickness >200 nm show better performance than the dense samples, while the situation is inversed for thinner films with the same thickness (<100 nm). Similar results are also obtained under back illumination (Figure S4, Supporting Information). Thus, to accurately evaluate the effect of pore structure, it is less than enough by just comparing two samples with the same thickness. The dense and the porous samples with best performance (marked with frames in Figure 2a) are used for comparison. The photoelectrochemical performance comparison between the dense and the porous samples with the same thickness (≈80 nm) is also discussed later in this work.

The incident photon to current efficiency (IPCE) of these two photoelectrodes is shown in Figure 2b. The porous structure photoelectrode has much higher IPCE than the planar electrode. Similar phenomena have been observed in previous works.[22,23] IPCE takes into account efficiencies for three fundamental processes which can be expressed by Equation (1).[24]

$$IPCE = \eta_{\text{abs}} \cdot \eta_{\text{sep}} \cdot \eta_{\text{int}} \tag{1}$$

Where η_{abs} is the light harvesting efficiency, η_{sep} is the separation efficiency for photo-generated carriers, and η_{int} is interfacial charge transfer efficiency. In order to identify quantitative contribution of each parameter in Equation (1) on the improved photocurrent, these processes should be decoupled and investigated separately.

2.2. Comparison of Light Absorption on a Solid/Electrolyte BHJ and a Planar Structure

Light harvesting efficiencies of the porous and the dense Mo doped $BiVO_4$ films in electrolyte were determined using an integrating sphere. **Figure 3** shows the reflection, transmission and absorption spectra of the porous and the dense Mo doped $BiVO_4$ films. The absorption edge of both the porous and the dense films is at about 510 nm, corresponding to a band gap of 2.4 eV. Compared to a dense film, pore structure enhances light harvesting by reducing the reflection and the transmission. Two reasons are responsible for higher light absorption of the porous sample. One is the different film thickness, the other is stronger light scattering in a porous sample. The porous film is recognized to enhance the light harvesting due to light scattering within the pores by increasing the optical path length of light, especially in the wavelength range corresponding to the band edge.[25–27] Light absorption of a porous film at 420 nm is 14% higher than that of a dense sample, while it is 140% higher at 480 nm. The results suggest that the porous structure can enhance light absorption more effectively near band edge region.

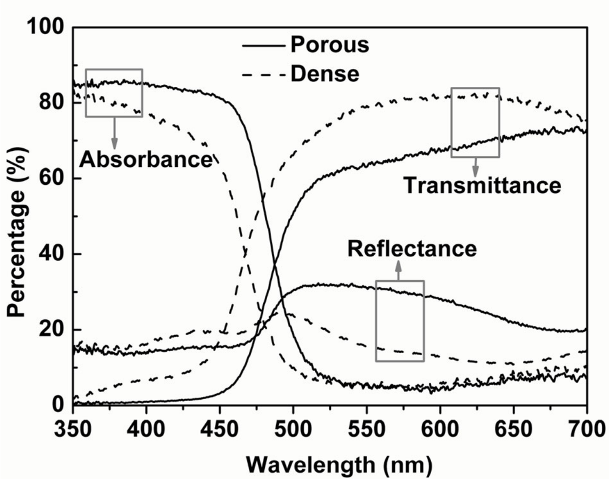

Figure 3. Absorption of the porous and the dense Mo doped $BiVO_4$ films in 0.5 M Na_2SO_4 aqueous solution by estimating transmission and reflection spectra using an integrating sphere (Absorbance = 1 – Transmittance – Reflectance). Measurement details are shown in Supporting Information for reflection and transmission spectroscopy measurements (Figure S5–S8).

To investigate other parameters' contribution to the enhanced photoelectrochemical performance, absorbed photon to current efficiency spectra (APCE), or internal quantum efficiency, is derived from Equation (2) to decouple the light absorption effect.

$$APCE = \frac{IPCE}{\eta_{\text{abs}}} = \eta_{\text{sep}} \cdot \eta_{\text{int}} \tag{2}$$

Figure 4 depicts the APCE spectra of the two samples. Internal quantum efficiency of the porous film is still much higher than that of the dense film after excluding the difference of light absorption. We also calculated the solar photocurrent by integrating IPCEs (Figure 2b) and APCEs (Figure 4) of the porous and the dense films with the standard solar spectrum following Gratzel's method.[13] The calculated solar photocurrent of the porous film is 2.1 times as high as that of the dense film at 1.23 V_{RHE} using IPCE data, while the calculated solar photocurrent of the porous film is 1.7 times as high as that of the dense film at 1.23 V_{RHE} using APCE data. Therefore, not light absorption, but other parameter plays a more important role in improving photoelectrochemical performance of the porous sample. The results are similar to a BHJ OPV, in which a much smaller pore size is used and negligible light scattering exist. However, a BHJ has higher performance than a planar structure.[6]

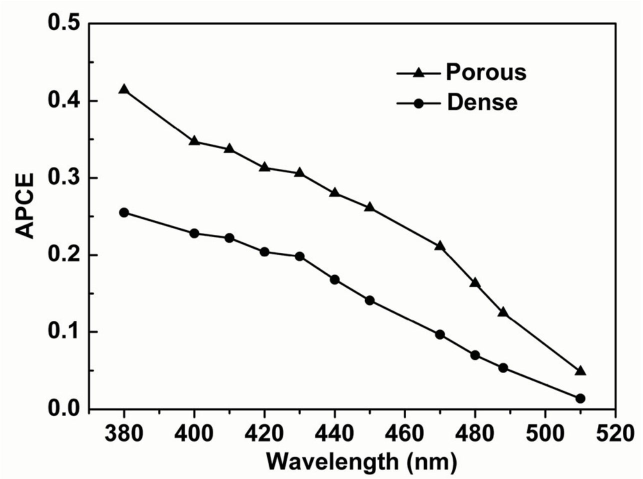

Figure 4. Absorbed photon to current efficiency (APCE) at 1.23 V_{RHE} of the porous and the dense Mo doped $BiVO_4$ films in 0.5 M Na_2SO_4 aqueous solution under front illumination.

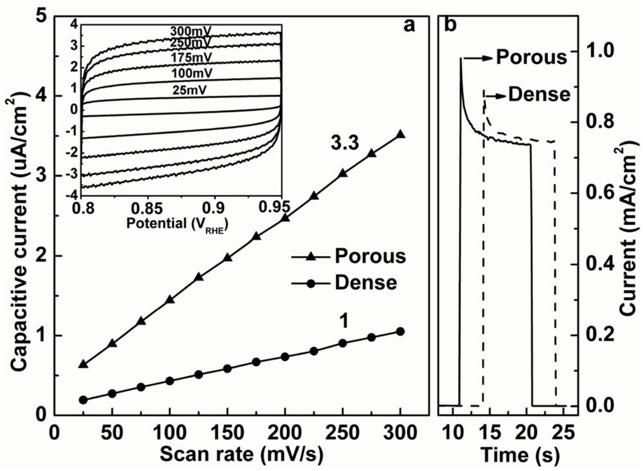

Figure 5. a) Relative electrochemical surface area measurement of the porous and the dense film: linear relationship between the capacitive current and scan rate for the porous and the dense film. The inset is the example cyclic voltammograms showing the capacitive current for the porous Mo doped $BiVO_4$ electrode at different scan rate from 25 to 300 mV s^{-1}. b) Transient photocurrent of the porous and the dense Mo doped $BiVO_4$ films at 1.23 V_{RHE} in 0.5 M Na_2SO_4 with light on and off. The same 10 s decayed photocurrents were obtained on the dense and the porous samples under illumination with different light intensity to obtain accurate comparison.

2.3. Comparison of Surface Recombination Processon a Solid/Electrolyte BHJ and a Planar Structure

The relative surface area of the porous and dense samples are determined from the capacitive current shown in **Figure 5**a.[16] The electrochemical surface area of the porous structure is 3 times as high as that of the dense sample, which arises from the penetration of electrolyte into pores of the porous film. Higher surface area means more surface trapping states, which is unfavorable to water oxidation due to the poor water oxidation kinetics.[28,29] As a consequence, there exists surface recombination. Herein, we investigate the surface recombination process in these two samples. Transient photocurrent is a good tool to gain information on surface recombination process.[29] As shown in Figure 5b, the photocurrent transient of the porous film is much more conspicuous than that of the dense film, which meansmore surface recombination in the porous film than that in the dense film.

Furthermore, the comparison of the photocurrents of thinner porous and the dense films (with the same thickness ≈80 nm) also shows more surface recombination in the porous film (**Figure 6**). In Figure 6a, the water oxidation photocurrent of the porous film (≈80 nm) is lower than that of the dense film (≈80 nm), which is also mentioned in Figure 2. However, a higher performance on the porous film than the dense one with the same thickness is observed (Figure 6b) after decoupling surface recombination by adding the hole scavenger H_2O_2, in the presence of which surface recombination is suppressed due to its rapid and facile oxidation.[30,31] The comparison of Figure 6a and 6b apparently shows that the porous film with larger surface area (Figure 6c) has lower interfacial charge transfer efficiency for water oxidation than the dense film.

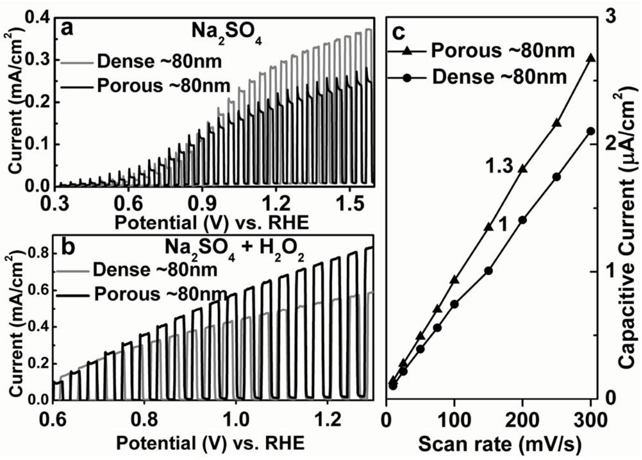

Figure 6. Photocurrents of the porous and the dense films with the same thickness (≈80 nm) in a) 0.5 M Na_2SO_4 and b) 0.5 M Na_2SO_4 together with 0.5 M H_2O_2 as hole scavenger with a 500 W Xe lamp equipped with a 420 nm cut-off filter at a scan rate of 30 mV s–1. c) Relative electrochemical surface area measurement: the linear relationship between the capacitive current and scan rate for the porous and the dense films with the same thickness (≈80 nm).

2.4. Comparison of Charge Separation Efficiency on a Solid/Electrolyte BHJ and a Planar Structure

The interfacial charge transfer efficiency η_{int} for the porous and the dense films is different, which can blur intrinsic transport properties of photo-generated carriers in the porous sample. Here, H_2O_2 is used to obtain the charge separation efficiency η_{sep} with $\eta_{\text{int}} = 1$ by completely suppressing surface recombination. Hence, according to Equation (2), APCE measured in H_2O_2 is the charge separation efficiency η_{sep}. **Figure 7** shows the charge separation efficiency for the porous and the dense films. For the dense film, the charge separation is much effective from front illumination than that from back illumination, which indicates poor hole transport property in the Mo doped $BiVO_4$. However, for a porous film, the charge separation efficiencies are almost the same under front and back illumination. The difference under front and back illumination for the porous and the dense films indicates different transport path for photo-generated holes in the porous and the dense samples, which will be discussed later. Moreover, the integral photocurrent of the porous film from APCE data (= charge separation efficiency) in H_2O_2 (Figure 7) is about 2 times as high as that of a dense film, which is almost the same with the integral photocurrent for water oxidation from IPCE in Figure 2b. These results, in consideration of the slightly enhanced light absorption and more serious surface recombination for water splitting, suggest that the enhanced water oxidation photocurrent of the Mo doped $BiVO_4$ electrode mainly comes from the effective charge separation.

Poor hole transport in the Mo doped $BiVO_4$ sample limits its photocurrent as mentioned above. In previous studies, pore structure permits electrolyte to penetrate in the film and shortens the transport distance for holes to the surface. However, no direct evidence is offered. In this work, we present visualized evidence to show higher charge separation

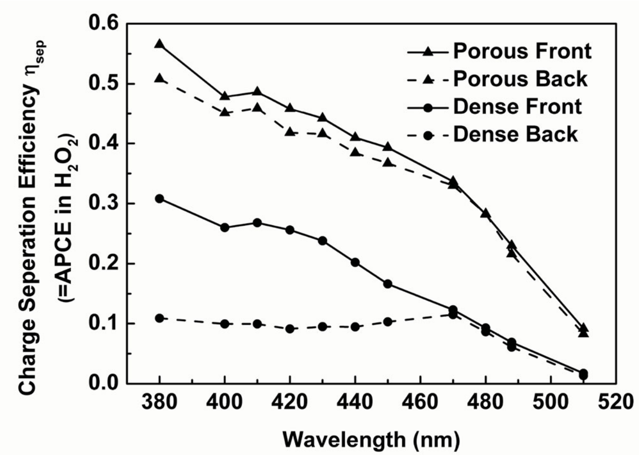

Figure 7. Charge separation efficiency at 1.23 V_{RHE} of the porous and the dense Mo doped $BiVO_4$ films measured in 0.5 M Na_2SO_4 together with 0.5 M H_2O_2 under front and back illumination in consideration of light absorption.

efficiency comes from a shorter holes diffusion distance in a solid-liquid bulk heterojunction by using Mn^{2+} as the photo-generated hole imaging agent.[32] The results can show the hole transport process visibly, since MnO_x will be deposited at the interface of the solid-liquid bulk heterojunction, where photo-generated holes reach. Photo-deposition of MnO_x on the surface of the $BiVO_4$ samples was performed at 1.1 V_{RHE} from backside illumination to show hole transport more clearly. The potential is lower than the electro-oxidation potential of Mn^{2+} in the dark (begins at 1.2 V_{RHE} in Figure S9). Thus, MnO_x are only oxidized by photo-generated holes. The amounts of MnO_x are the same by controlling the same electricity quantity (≈4 mC). In **Figure 8**a, large amounts of MnO_x are grown on the top of the dense film, while much less MnO_x are observed on the top of the porous film (Figure 8b). From cross-section SEM images of the dense and the porous films in Figure 8c and 8d, MnO_x are merely deposited on the top of the compact $BiVO_4$ layer, while MnO_x deposited uniformly on the surface of each $BiVO_4$ particles of the porous sample. The observation of different MnO_x deposition sites clearly shows different transport path for photo-generated holes in the porous and the dense samples as mentioned above. This is the visualized evidence for shorter hole diffusion distance in a solid-liquid BHJ than a planar structure, which can also be used to understand the interface charge transfer process in a BHJ OPV. According to above analysis, a sketch for different transport process of photo-generated carriers in the porous and the dense samples is demonstrated in **Figure 9**.

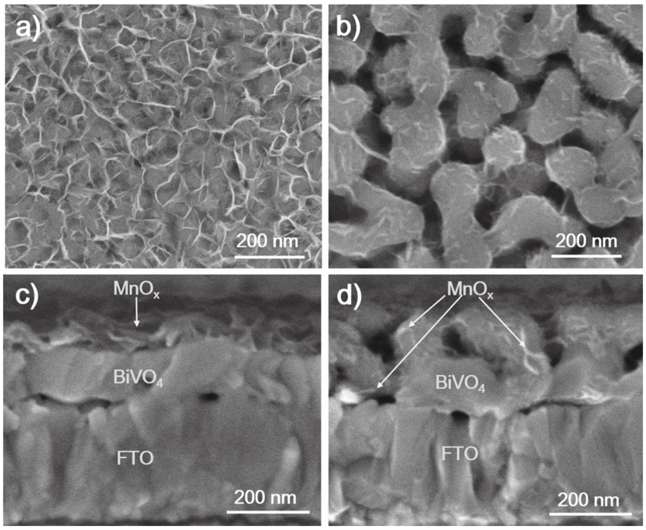

Figure 8. Top view SEM images of a) a dense Mo doped $BiVO_4$ film after photo-deposition of Mn^{2+}, b) a porous Mo doped $BiVO_4$ film after photo-deposition of Mn^{2+}, and cross-section SEM images of c) a dense Mo doped $BiVO_4$ film after photo-deposition of Mn^{2+}, d) a porous Mo doped $BiVO_4$ film after photo-deposition of Mn^{2+}.

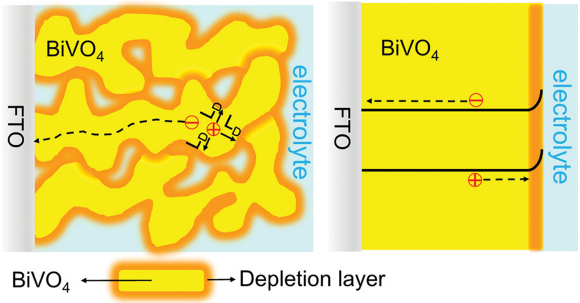

Figure 9. Illustration of charge separation of the porous and the dense Mo doped $BiVO_4$ films.

2.5. Insight into Designing a Better Performance Solid/Liquid BHJ

Though the solid/liquid BHJ has enhanced charge separation efficiency very much, the values are still low, less than 60% at 1.23 V_{RHE}. Recently, a record solar-to-hydrogen efficiency of 4.9% in $BiVO_4$ has been reported by Krol and coworkers.[33] However, the charge separation efficiency at 1.23 V_{RHE} is about 60%. There is much room to improve the charge separation efficiency. Here, the limit for low charge separation efficiency is analyzed. In a highly doped $BiVO_4$, the depletion layer width is estimated as 3.5 nm (see Supporting Information Equation S2). Therefore, diffusion is the main mechanism for charge separation. The hole diffusion length L_D of the Mo doped $BiVO_4$ is calculated as about 20 nm (see Supporting Information Equation S3). It is noted that a hole diffusion length of ~100 nm was reported in W:$BiVO_4$,[34] and $BiVO_4$ single crystals,[35] which mainly arises from different measured absorption coefficient and preparation method of the samples. However, the $BiVO_4$ particle size in the porous sample is over 100 nm. Not all the photo-generated holes in the particle can diffuse to the solid/liquid interface. The relatively large particle size limits the photoelectrochemical performance. If the particle size is less than $2L_D$, the porous films would have higher charge separation efficiency (see Figure 9). Therefore, a porous $BiVO_4$ electrode with a smaller particle size is preferred to further improve the photocurrent.

3. Conclusions

Comparable samples of the porous and the dense Mo doped $BiVO_4$ films have been successfully prepared in this study. Solid/liquid bulk heterojunction and planar cells have been obtained in porous and dense samples, respectively. Higher photoelectrochemical properties are obtained in the porous $BiVO_4$ sample. Improved performance in the porous sample comes from higher light absorption and higher charge separation efficiency. The quantitative analysis suggests charge separation efficiency have a more important role than light absorption. Moreover, visualized evidence is given to show higher charge separation efficiency comes from a shorter photo-generated holes diffusion distance in a solid/liquid BHJ. A porous $BiVO_4$ electrode with a smaller particle size ($2L_D$) is preferred to further improve the photocurrent. The concept can be applied to improving the performance of other low cost photoconversion devices due to similar processes of carrier separation.

4. Experimental Section

Preparation of Dense and Porous Films: Mo doped $BiVO_4$ photoelectrodes were fabricated by metal-organic decomposition method based on our previous work.[36] $Bi(NO_3)_3{\cdot}5H_2O$ in glacial acetic acid (0.2 mol L^{-1}), vanadylacetyl acetonate in acetylacetone (0.03 mol L^{-1}) and Molybdenyl acetylacetonate in acetylacetone (0.01 mol L^{-1}) were used as starting solutions. Proper amount of these solutions were well mixed together according to the stoichiometric ratio of Bi : V : Mo as 100 : 97 : 3, then dropped on FTO substrates (1 $cm^2 \times 1.5$ cm^2), dried and then calcined at 470 °C in a muffle furnace for 30 min to form $BiVO_4$:Mo films. Porous thin films of different thickness were obtained by dropping one layer of the mixed solution on the FTO substrates with different volumes (15–55 µL), followed by drying and then calcining at 470 °C for 30 min. Thicker films cannot be achieved by dropping more solution, due to extravasation of solution from the FTO. For a dense film, a main difference is to change volume and dropping layers. For each layer, much less solution (2.5 µL) was dropped and calcined, and different thickness was obtained by repeating the above procedure. All the samples were finally calcined at 470 °C for 5 h to exclude the influence of the crystallinity.

Characterization of Samples: The morphologies of the $BiVO_4$ films were imaged by scanning electron microscopy (SEM) (Nova NanoSEM 230, FEI Co.). Film thickness was estimated by AFM (MFP3D microscope Asylum Research, MFP-3D-SA, USA) and a Dektak Series150 Surface Profiler. The light harvesting efficiency was obtained by measuring the reflectance and transmittance using UV-visible spectrophotometer with an integrating sphere (Shimadzu, UV-2550, Japan). The measurement details for light harvesting efficiency are shown in Supporting Information. Crystallinity was identified by X-ray diffraction (XRD) patterns (Ultima III, Rigaku) with Cu Kα radiation ($\lambda = 0.154$ nm). The chemical states of Mo ions in doped BiVO4 were investigated by X-ray photoelectron spectroscopy (XPS, Thermo ESCALAB 250). The binding energy was calibrated by C1s (284.6 eV). The Raman spectra at room temperature were measured by a Laser Raman spectrophotometer (JY-HR800).

Photoelectrochemical and Electrochemical Measurements: Photoelectrochemical measurements were performed in a three-electrode setup (CHI-633C, Shanghai Chenhua, China), with a photoanode as a working electrode, a Pt foil as a counter electrode and a saturated calomel electrode as a reference electrode. All the samples were pretreated following the method reported by us.[37] A light source for photoelectrochemical measurements was a 500 W xenon lamp equipped with a 420 nm cut-off filter when necessary. The 420 nm cut-off filter is used to exclude the absorption difference from front and back illumination, considering the FTO absorption (<400 nm). The water splitting photocurrents were measured in 0.5 M Na_2SO_4 aqueous solution (pH = 6) at a scan rate of 30 mV/s. Charge separation efficiency was obtained by measuring light absorption and photocurrents in 0.5 M Na_2SO_4 + H_2O_2 aqueous solution. Potentials of the working electrode were given on RHE scale to easily compare with other results from the following formula:

$$V_{RHE} = V_{sc} + 0.059pH + 0.24 \tag{3}$$

where V_{RHE} is a potential versus a reversible hydrogen potential, V_{sc} is a potential versus saturated calomel electrode, and pH is a pH value of the electrolyte. The incident photon to current efficiency (IPCE) was performed under monochromatic light using bandpass filters. IPCE was calculated as follows,

$$IPCE = \frac{1240(\mathrm{V \cdot nm}) \cdot i(\mathrm{mA/cm^2})}{P_\lambda(\mathrm{mW/cm^2}) \cdot \lambda(\mathrm{nm})} \tag{4}$$

where 1240 (V nm) is a multiplication of h (Planck's constant) and c (the speed of light), i (µA cm^{-2}) is the photocurrent density, λ (nm) is the wavelength, and $P\lambda$ (µW cm^{-2}) is the light intensity at λ. $P\lambda$ was measured with a photometer (Newport, 840-C, USA). The photocurrent density, i, was determined by measuring current versus time curve at a constant potential (1.23 V_{RHE}).

The photo-oxidation of Mn^{2+} was achieved also in the three-electrode setup in 0.5 M Na_2SO_4 aqueous solution together with 0.01 M $MnSO_4$ at 1.1 V_{RHE} under back illumination. The quantity of electricity was ~4 mC.

The relative surface areas of the samples were determined by capacitive current between 0.8 V_{RHE} and 0.95 V_{RHE} in 0.5 M Na_2SO_4 aqueous solution in the dark.[16] The scan rate was changed from 25 to 300 mV s^{-1}.

Supporting Information

Supporting Information is available from the Wiley Online Library or from the author.

Acknowledgements

This work is supported by the National Basic Research Program of China (973 Program, 2013CB632404 and 2014CB239303), the National Natural Science Foundation of China (51272101, 11174129) and the Jiangsu Provincial Natural Science Foundation (No.BK20130053) and Jiangsu key laboratory for nanotechnology.

Received: November 21, 2013
Revised: December 27, 2013

[1] A. J. Heeger, *Chem. Soc. Rev.* **2010**, *39*, 2354.
[2] S. W. Boettcher, J. M. Spurgeon, M. C. Putnam, E. L. Warren, D. B. Turner-Evans, M. D. Kelzenberg, J. R. Maiolo, H. A. Atwater, N. S. Lewis, *Science* **2010**, *327*, 185.
[3] A. Fujishima, K. Honda, *Nature* **1972**, *238*, 37.
[4] Z. Li, W. Luo, M. Zhang, J. Feng, Z. Zou, *Energy Environ. Sci.* **2013**, *6*, 347.
[5] M. Li, W. Luo, D. Cao, X. Zhao, Z. Li, T. Yu, Z. Zou, *Angew. Chem. Int. Ed.* **2013**, *52*, 11016.
[6] G. Yu, J. Gao, J. Hummelen, F. Wudl, A. Heeger, *Science* **1995**, *270*, 1789.
[7] S. H. Park, A. Roy, S. Beaupré, S. Cho, N. Coates, J. S. Moon, D. Moses, M. Leclerc, K. Lee, A. J. Heeger, *Nat. Photon.* **2009**, *3*, 297.

[8] G. Li, R. Zhu, Y. Yang, *Nat. Photon.* **2012**, *6*, 153.
[9] M. D. Kelzenberg, S. W. Boettcher, J. A. Petykiewicz, D. B. Turner-Evans, M. C. Putnam, E. L. Warren, J. M. Spurgeon, R. M. Briggs, N. S. Lewis, H. A. Atwater, *Nat. Mater.* **2010**, *9*, 239.
[10] K. Shankar, J. I. Basham, N. K. Allam, O. K. Varghese, G. K. Mor, X. Feng, M. Paulose, J. A. Seabold, K.-S. Choi, C. A. Grimes, *J. Phys. Chem. C* **2009**, *113*, 6327.
[11] M. Law, J. Goldberger, P. Yang, *Annu. Rev. Mater. Res.* **2004**, *34*, 83.
[12] T. J. Kempa, R. W. Day, S.-K. Kim, H.-G. Park, C. M. Lieber, *Energy Environ. Sci.* **2013**, *6*, 719.
[13] A. Kay, I. Cesar, M. Grätzel, *J. Am. Chem. Soc.* **2006**, *128*, 15714.
[14] I. S. Cho, Z. Chen, A. J. Forman, D. R. Kim, P. M. Rao, T. F. Jaramillo, X. Zheng, *Nano Lett.* **2011**, *11*, 4978.
[15] B. D. Alexander, P. J. Kulesza, L. Rutkowska, R. Solarska, J. Augustynski, *J. Mater. Chem.* **2008**, *18*, 2298.
[16] B. A. Pinaud, P. C. Vesborg, T. F. Jaramillo, *J. Phys. Chem. C* **2012**, *116*, 15918.
[17] M. Grätzel, *Nature* **2001**, *414*, 338.
[18] C. Santato, M. Odziemkowski, M. Ulmann, J. Augustynski, *J. Am. Chem. Soc.* **2001**, *123*, 10639.
[19] W. Luo, Z. Yang, Z. Li, J. Zhang, J. Liu, Z. Zhao, Z. Wang, S. Yan, T. Yu, Z. Zou, *Energy Environ. Sci.* **2011**, *4*, 4046.
[20] K. S. Choi, *J. Phys. Chem. Lett.* **2010**, *1*, 2244.
[21] G. Yuan, K. Aruda, S. Zhou, A. Levine, J. Xie, D. Wang, *Angew. Chem. Int. Ed.* **2011**, *50*, 2334.
[22] M. J. Price, S. Maldonado, *J. Phys. Chem. C* **2009**, *113*, 11988.
[23] L. W. Zhang, Y. J. Wang, H. Y. Cheng, W. Q. Yao, Y. F. Zhu, *Adv. Mater.* **2009**, *21*, 1286.
[24] Z. Chen, T. F. Jaramillo, T. G. Deutsch, A. Kleiman-Shwarsctein, A. J. Forman, N. Gaillard, R. Garland, K. Takanabe, C. Heske, M. Sunkara, *J. Mater. Res.* **2010**, *25*, 3.
[25] M. Gratzel, *J. Photoch. Photobio. A* **2004**, *164*, 3.
[26] X. Chen, J. Ye, S. Ouyang, T. Kako, Z. Li, Z. Zou, *Acs Nano* **2011**, *5*, 4310.
[27] Z. P. Tian, H. M. Tian, X. Y. Wang, S. K. Yuan, J. Y. Zhang, X. B. Zhang, T. Yu, Z. G. Zou, *Appl. Phys. Lett.* **2009**, *94*, 031905.
[28] F. Le Formal, N. Tétreault, M. Cornuz, T. Moehl, M. Grätzel, K. Sivula, *Chem. Sci.* **2011**, *2*, 737.
[29] F. Le Formal, K. Sivula, M. Gratzel, *J. Phys. Chem. C* **2012**, *116*, 26707.
[30] K. Itoh, J. M. Bockris, *J. Electrochem. Soc.* **1984**, *131*, 1266.
[31] H. Dotan, K. Sivula, M. Grätzel, A. Rothschild, S. C. Warren, *Energy Environ. Sci.* **2011**, *4*, 958.
[32] R. G. Li, F. X. Zhang, D. G. Wang, J. X. Yang, M. R. Li, J. Zhu, X. Zhou, H. X. Han, C. Li, *Nat. Commun.* **2013**, *4*, 1432.
[33] F. F. Abdi, L. Han, A. H. M. Smets, M. Zeman, B. Dam, R. van de Krol, *Nat. Commun.* **2013**, *4*, 2195.
[34] D. K. Zhong, S. Choi, D. R. Gamelin, *J. Am. Chem. Soc.* **2011**, *133*, 18370.
[35] A. J. Rettie, H. C. Lee, L. G. Marshall, J.-F. Lin, C. Capan, J. Lindemuth, J. S. McCloy, J. Zhou, A. J. Bard, C. B. Mullins, *J. Am. Chem. Soc.* **2013**, *135*, 11389.
[36] W. Luo, J. Wang, X. Zhao, Z. Zhao, Z. Li, Z. Zou, *Phys. Chem. Chem. Phys.* **2013**, *15*, 1006.
[37] W. Luo, Z. Li, T. Yu, Z. Zou, *J. Phys. Chem. C* **2012**, *116*, 5076.